

Study on irradiation effects of refractory bcc high-entropy alloy

Yun Zong^{a,*}, Naoyuki Hashimoto^b, Hiroshi Oka^b

^a Graduate School of Engineering, Hokkaido University, Hokkaido 060-8628, Japan

^b Faculty of Engineering, Hokkaido University, Hokkaido 060-8628, Japan



ARTICLE INFO

Keywords:

Irradiation hardening
High entropy alloy
Mechanical properties

ABSTRACT

We developed body-centered cubic refractory high-entropy alloys, MoNbTaTi, MoNbTaW, and MoNbTaTiW, and explored their microstructure, and mechanical properties in order to develop a new high-irradiation resistance material suitable for fusion reactor components. Three HEAs were annealed at 1200 °C for 48 h to form single face BCC alloys, while MoNbTaW was also annealed at 1500 °C. SEM inspection and EDS mapping have both validated this result. The Vickers hardness of three HEAs was investigated, and the stable results indicate that they are all stable at elevated temperatures. Three HEAs are ion irradiated with 6.4 MeV Fe³⁺ at a temperature of 500 °C, and the irradiation hardening is examined using nanoindentation. In comparison to pure tungsten, the three HEAs exhibit increased resistance to irradiation.

Introduction

As is well known, conventional alloys contain the primary element, comprising around 80% to 90% of the alloy composition. Even superalloys, which contain 12 elements, also contain a minimum of 50% of the primary elements. [1] Researchers have recently proposed high entropy alloys (HEA), which have garnered considerable attention as a potential material. According to Yeh's composition-defined definition, HEAs comprise four or more elements in equimolar or near-equimolar proportions, with element concentrations ranging from 5% to 35%. [2–5] The entropy-based definition defines the HEA as having the highest potential entropy, implying that such a state is achievable at extremely high temperatures or in the liquid form. Researchers hypothesized that HEAs had a complex element composition but a simple structure based on their high-entropy effect. Additionally, it has been demonstrated that certain HEAs exhibit excellent mechanical properties from cryogenic to high temperatures. [6–8].

The materials applied in fusion reactors are subjected to tremendous heat flow and high-energy particles, necessitating materials with excellent thermal conductivity and irradiation resistance. According to the literature, candidates for fusion reactor refractory metals include Ta and Mo alloys due to their superior high-temperature strength and ductility. [9] Additionally, W has attracted significant emphasis as an ideal material for in-vessel components such as diverters and blankets in

a fusion reactor because of its high-temperature capabilities and low sputtering yield. However, tungsten's inherent brittleness at low temperatures and irradiation embrittlement have precluded its usage in fusion reactor applications. [10,11] Considering this, some investigations have focused on using HEAs in place of tungsten. Because the ductility of the Ti element is more significant than that of the refractory components (W, Ta). Ti was added to the HEAs to improve their properties. Corrosion resistance is required for the material used in fusion reactors. Although Mo and Nb are not low activation elements, they are typical elements that improve the corrosion resistance of stainless steel and other superalloys. [12–15] Therefore, refractory HEAs (which contain Ti, Zr, Hf, Ta, V, Nb, W, and Cr) are one type of contender because they display exceptional high melting points, ductility, and strength at elevated temperatures. [16–19] The microstructure and irradiation hardening of three HEAs (MoNbTaTi, MoNbTaW, and MoNbTaTiW) were examined in this work as part of the development of HEAs suitable for fusion reactors.

Experimental procedure

To fabricate three body-centered cubic high-entropy alloys, pure tungsten, niobium, titanium, tantalum, and molybdenum (>99.9 percent purity) were used as raw elements material. All HEAs (MoNbTaTi, MoNbTaW, and MoNbTaTiW) were made by arc-melting under a

* Corresponding author.

E-mail addresses: y-zong@eng.hokudai.ac.jp (Y. Zong), hasimoto@eng.hokudai.ac.jp (N. Hashimoto), hiroshi_oka@eng.hokudai.ac.jp (H. Oka).

Table 1

Chemical composition of MoNbTaW, MoNbTaTi, MoNbTaTiW produced by vacuum arc melting tested with XRF.

at(%)	W	Nb	Ta	Ti	Mo
MoNbTaTi	—	21.88	28.17	25.52	25.15
MoNbTaW	25.57	23.21	27.45	—	25.57
MoNbTaTiW	17.87	23.11	18.80	17.24	22.98

high vacuum, with the buttons turned and heated more than four times to achieve complete melting of all specimens. **Table 1** contains the chemical compositions of the three alloys found using an ED-XRF (Energy Dispersive X-Ray Fluorescence) spectrometer. All ingots were solution-annealed at 1200 °C to achieve homogeneously. The phase diagrams were calculated in **Fig. 1** with the CALPHAD methodology. CALPHAD methodology is a phenomenological approach for calculating/predicting thermodynamic, kinetic, and other properties of multicomponent materials systems. [20] Because MoNbTaW has a higher melting point than the other two HEAs, 1500 °C annealing is also used. **Table 2** contains the solution annealing conditions for the three alloys. The microstructures of the alloys were studied using a scanning electron microscope (SEM, JSM-6510LA) equipped with a 15 kV accelerating voltage energy dispersive spectrometer (EDS). The crystal structure of the annealed specimens was determined by X-ray diffraction (SmartLab XRD) with Cu K radiation at a speed of 6°/min. The hardness of the samples was determined at room temperature using a Vickers indenter (Struers) with a force of 1 kg and a dwell period of 15 s.

The specimens were irradiated at Kyoto University's dual-beam irradiation experimental test facility (DuET). Three HEAs were irradiated with 6.4 MeV Fe³⁺ ions at a concentration of 3.06×10^{19} ions/m² at a flux of 8.50×10^{15} ions/m²/s and at a temperature of 500 °C. The depth profile of displacement damage calculated using the stopping and range of ions in the matter (SRIM) package is depicted in **Fig. 2**. [21–23] To investigate the performance of irradiation hardening, a nano-indentation test was conducted using a nanoindenter (Agilent Technologies Inc. Model Nano Indenter G200) with a Berkovich-type indentation tip. Moreover, indentation was performed on the irradiation surface in the direction parallel to the incident Fe³⁺ beam. The constant stiffness measurement (CSM) technique was used to obtain the depth profile of the hardness [24].

Results and discussions

Analysis of the microstructure

Table 1 contains the chemical compositions of the three alloys with XRF, and the results indicate that all the as-cast alloys are close to homogeneous. According to **Fig. 1**, the phase diagram shows MoNbTaTi (A-Ti) and MoNbTaW (A-W) are single BCC alloys from room temperature to the melting point. In contrast, the phase diagram for MoNbTaTiW(A-TiW) is unstable from room temperature to 400 °C with bcc and hcp phases. **Fig. 4** shows Typical SEM-BEC images of as-cast alloys and indicates no contrast in all three alloys. However, the EDS mapping result for as-cast A-TiW (**Fig. 5**) indicates that the material consists of two phases, each of which contains five elements. This EDS mapping result is constituent with the phase diagram mentioned above. Therefore, high-temperature heat treatment is required for refractory HEAs. Three HEAs become single-phase alloys following heat treatment at 1200 °C; the phase results are also evaluated using XRD. The diffraction peaks of MoNbTaTi, MoNbTaW, and MoNbTaTiW after annealing are shown in **Fig. 3**. The diffraction peaks of three HEAs were identical to those of the single-phase BCC alloys. As indicated in **Figs. 6 and 7**, the BEC pictures for three refractory HEAs after 1200°C annealing or 1500°C annealing also demonstrate its high-temperature stability, as no phase shift occurs

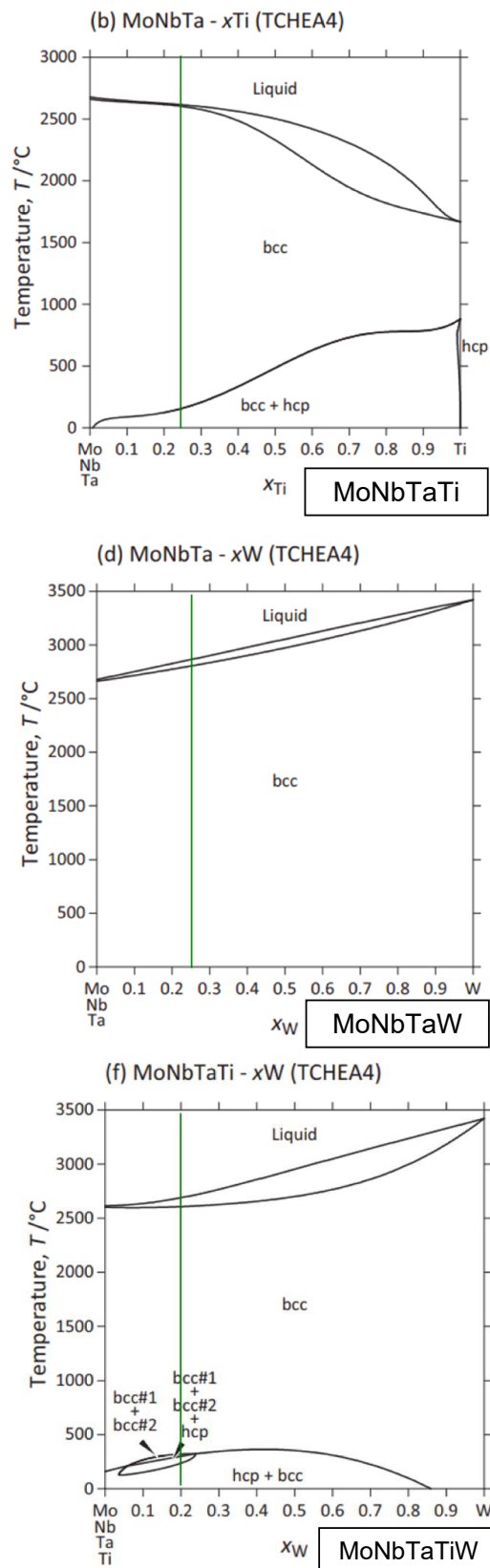


Fig. 1. Phase diagram for three refractory HEAs.

Table 2

Solution annealing conditions of refractory bcc high-entropy alloys.

Heat treatment condition	
MoNbTaW (A-W)	1200°C/48 h and 1500°C/48 h
MoNbTaTi (A-Ti)	1200°C/48 h
MoNbTaTiW (A-TiW)	1200°C/48 h

during annealing. Compared with other conventional alloys, this microstructure study indicated that high-entropy alloys had a simple microstructure despite their complex element constituents.

Mechanical properties

Vickers hardness values for three HEAs are shown in Fig. 8 before and after annealing. Vickers hardness values for annealed alloys were nearly identical to those for as-cast alloys. While A-W has a higher hardness than A-Ti and A-TiW, this is due to the higher hardness of pure tungsten in comparison to pure titanium. Additionally, the hardness of A-TiW is greater than that of A-Ti; this is owing to the typical hardening effect of solid solutions. It should be noted that the hardness of three HEAs was significantly higher (A-W: 550 Hv, A-Ti: 420 Hv, and A-TiW: 479 Hv) than that of pure tungsten (260–320 HV), which would be used for the International Thermonuclear Experimental Reactor's high heat flux components (ITER).

The result of nano-indentation

Fig. 9 illustrates the indentation depth profiles of three HEAs in the direction parallel to the incoming Fe^{3+} beam before and after ion irradiation, matching their nano-indentation hardness. The indentation size effect was found for all specimens, and the assessed hardness decreased with increasing indentation depth. Hardness fluctuations occurred at a depth of 400 nm in irradiated specimens, showing that the region of indentation-induced deformation extended to the boundary between the irradiated and unirradiated regions. Fig. 10 illustrates the Nix-Gao model for three HEAs, demonstrating that A-Ti and A-TiW exhibit evident irradiation hardening, whereas A-TiW exhibits less irradiation hardening than A-Ti. This could be related to the high-entropy effect, which states that increasing entropy can stabilize a phase with a greater entropy at elevated temperatures. Because the nano-indentation result is unreliable below 100 nm, the nano-indentation hardness at 350 nm was used to compare the pre-and post-irradiation stages. Fig. 11 illustrates the results of irradiation hardening on the alloy and recrystallized pure W [25], both of which were irradiated with 6.4 MeV Fe^{3+} ions at the same ion irradiation facility (DuET). Zhang et al. explored irradiation hardening using a Nix-Gao equation-based approach. The nano-indentation hardness at 350 nm was chosen for comparison with our findings, and the irradiation hardening was displayed. Fig. 11 demonstrates that the irradiation hardening of three HEAs is less than that of pure tungsten, implying that refractory BCC HEAs are more resistant to irradiation than pure tungsten. Besides the high-entropy effect, the high-entropy alloys also have the cocktail effect; their properties are certainly related to the properties of their compositing elements, which may also increase their mechanical properties, high-temperature behavior, and irradiation resistance.

Summary

Refractory high-entropy alloys: MoNbTaW, MoNbTaTi, MoNbTaTiW were produced by vacuum arc melting with pure metals and irradiated by DUET with 6.4 MeV Fe^{3+} at 500°C.

After heat treatment at 1200 °C or 1500 °C, the three HEAs transformed into single-phase bcc alloys. The average Vickers hardness of three alloys was almost the same after annealing at 1500 °C or 1200 °C,

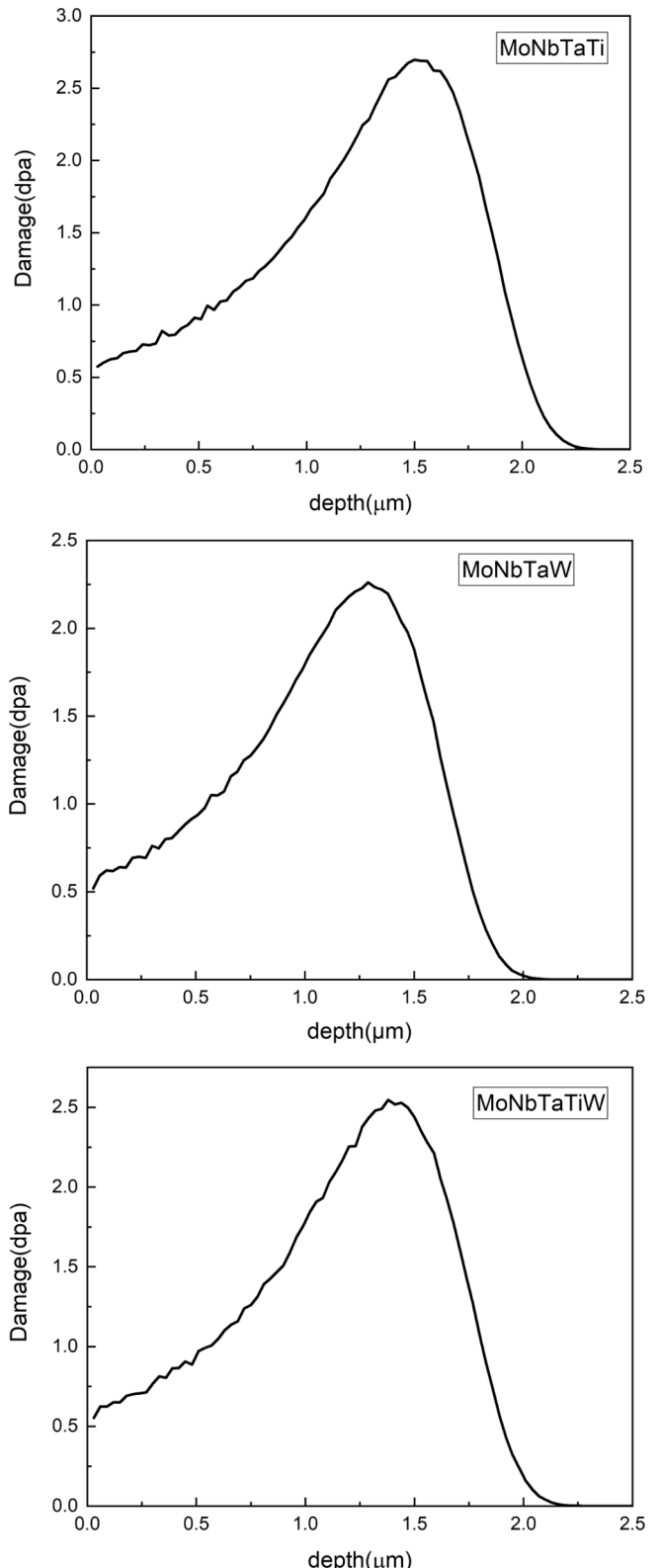


Fig. 2. Depth profile of displacement damage (dpa) induced by irradiation with 6.4 MeV Fe^{3+} .

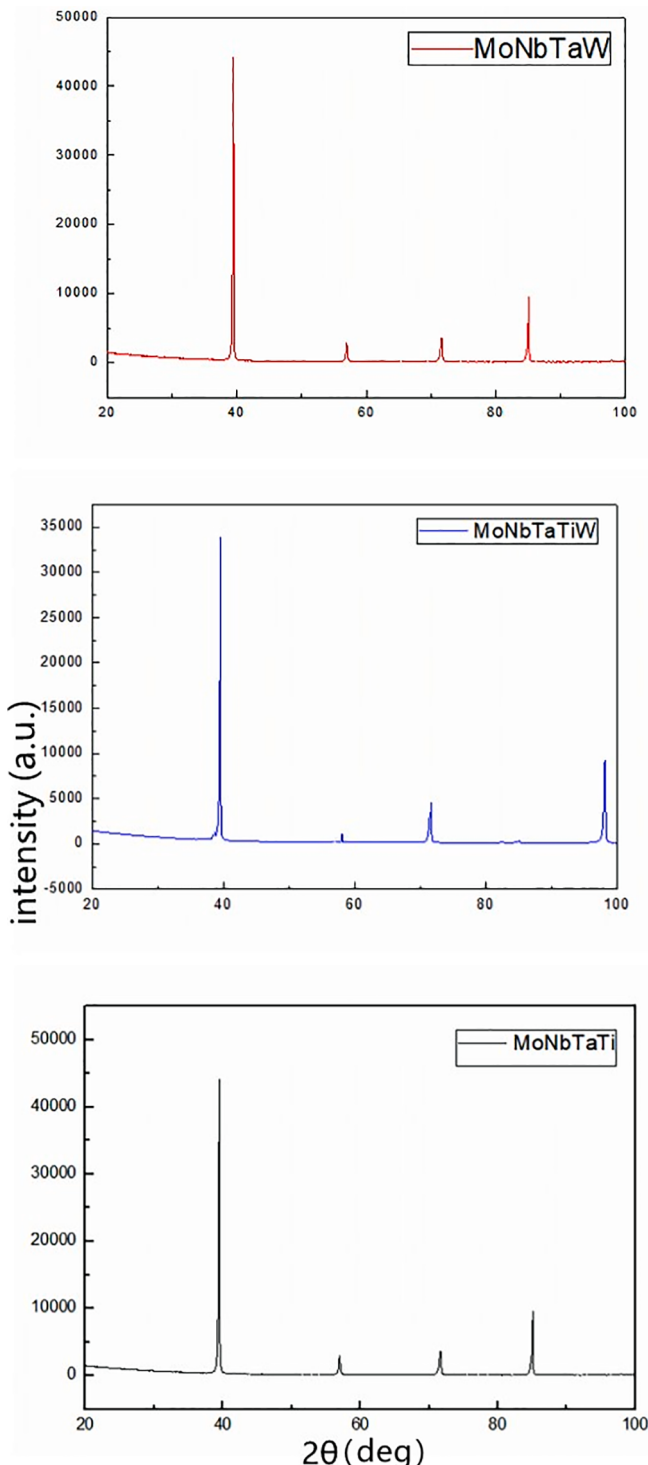


Fig. 3. XRD patterns for the Co-free Cu-containing solid solution concentrated alloys.



Fig. 4. Typical SEM-BEC images of as-cast alloys.

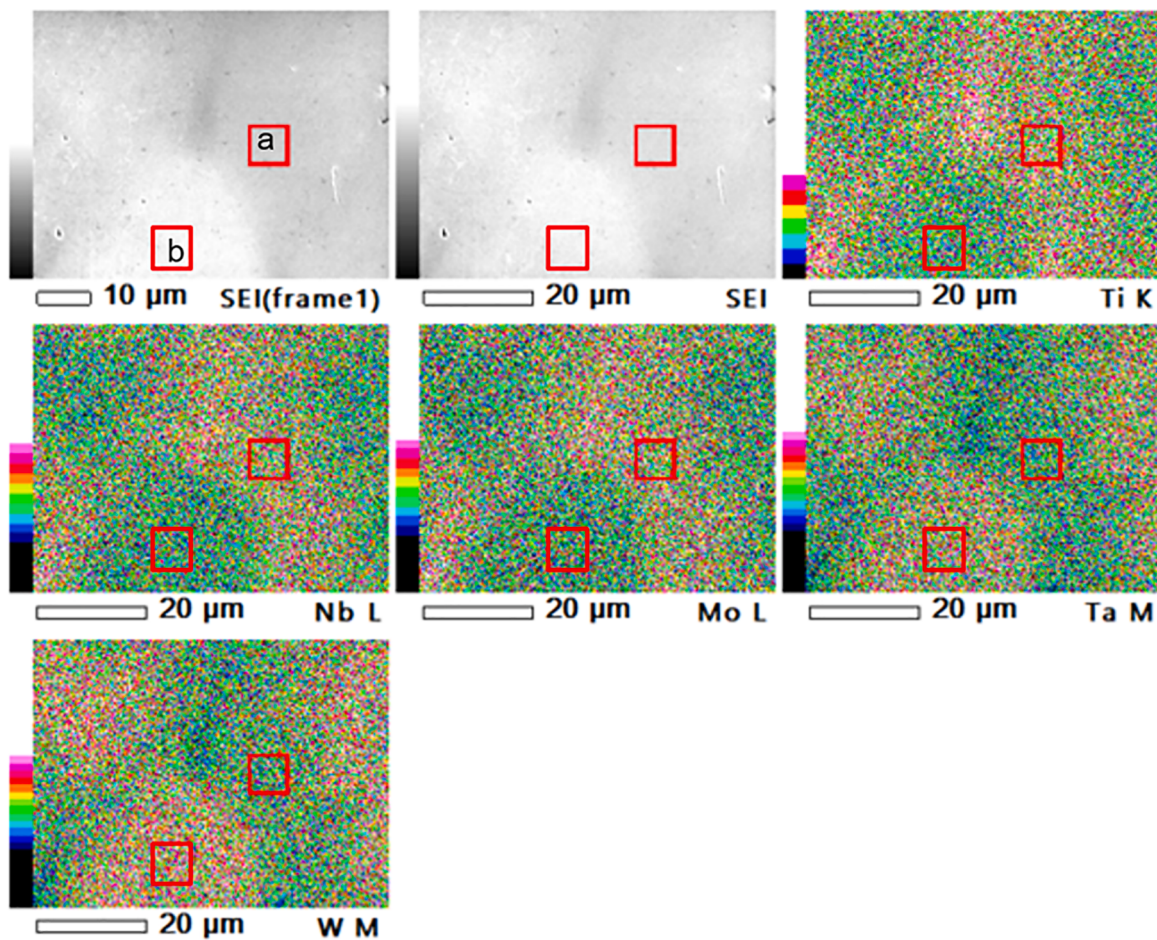


Fig. 5. EDS-mapping image of MoNbTaTiW.

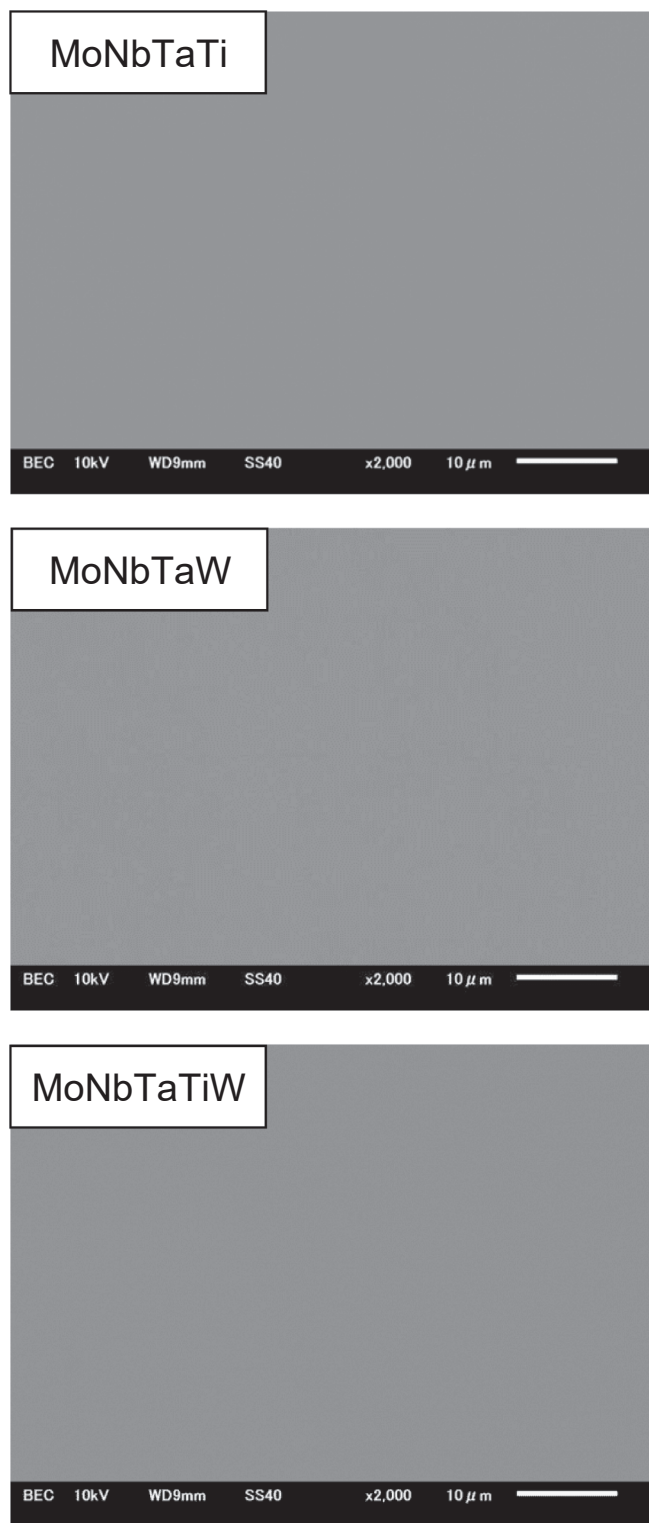


Fig. 6. Typical SEM-BEC images of annealed alloys (1200°C, 48 h).

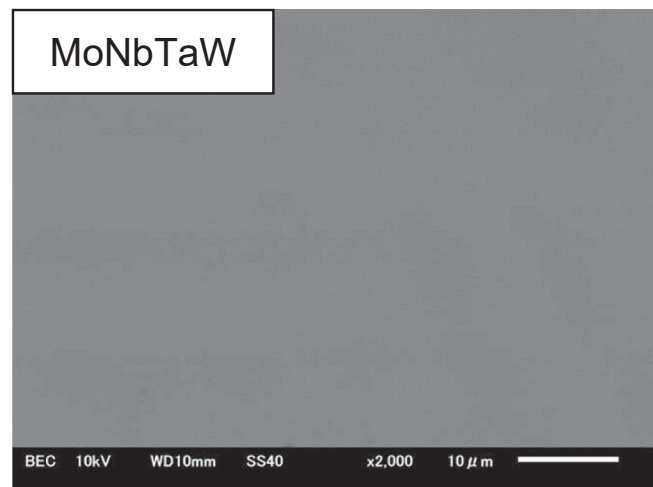


Fig. 7. Typical SEM-BEC images of MoNbTaW after 1500°C, 48 h heat-treatment.

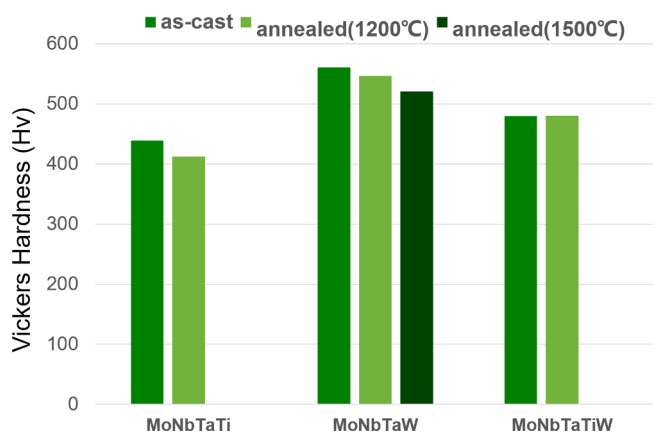


Fig. 8. Vickers hardness of all the alloys of as-cast and solution annealed for 48 h.

indicating that they exhibit high-temperature stability (MoNbTaW: 550 Hv, MoNbTaTi: 420 Hv, MoNbTaTiW: 479 Hv). From the Nix-Gao model result, the irradiation hardening of MoNbTaTiW is less than that of MoNbTaTi, possibly because of the high entropy effect. There is no noticeable irradiation hardening of MoNbTaW. At a depth of 350 nm, the irradiation hardening of MoNbTaTi and MoNbTaTiW was less than that of pure W. (peak region). Additional TEM observations of irradiated specimens and analysis of the nano-indentation result and TEM image will be required.

CRediT authorship contribution statement

Yun Zong: Methodology, Data curation, Writing – original draft, Writing – review & editing. **Naoyuki Hashimoto:** Supervision. **Hiroshi Oka:** Writing – review & editing.

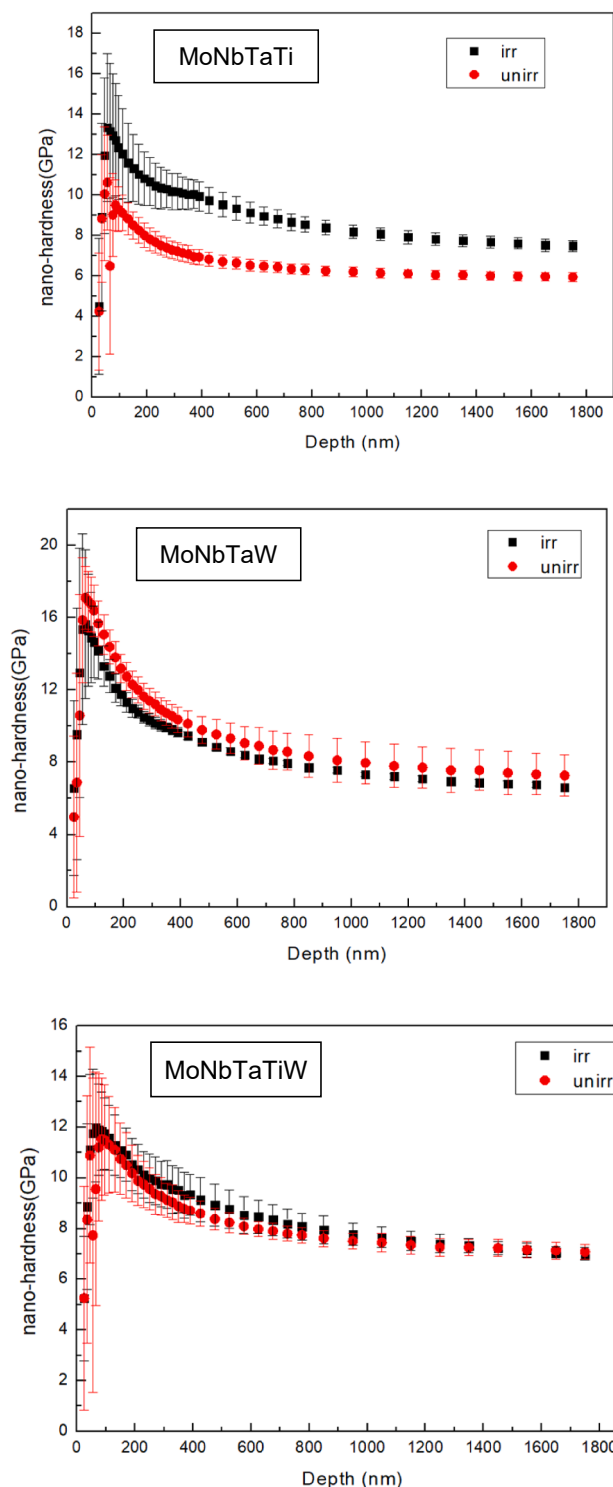


Fig. 9. Depth profiles of nanohardness in the direction parallel to the incident Fe^{3+} beam before and after ion irradiation.

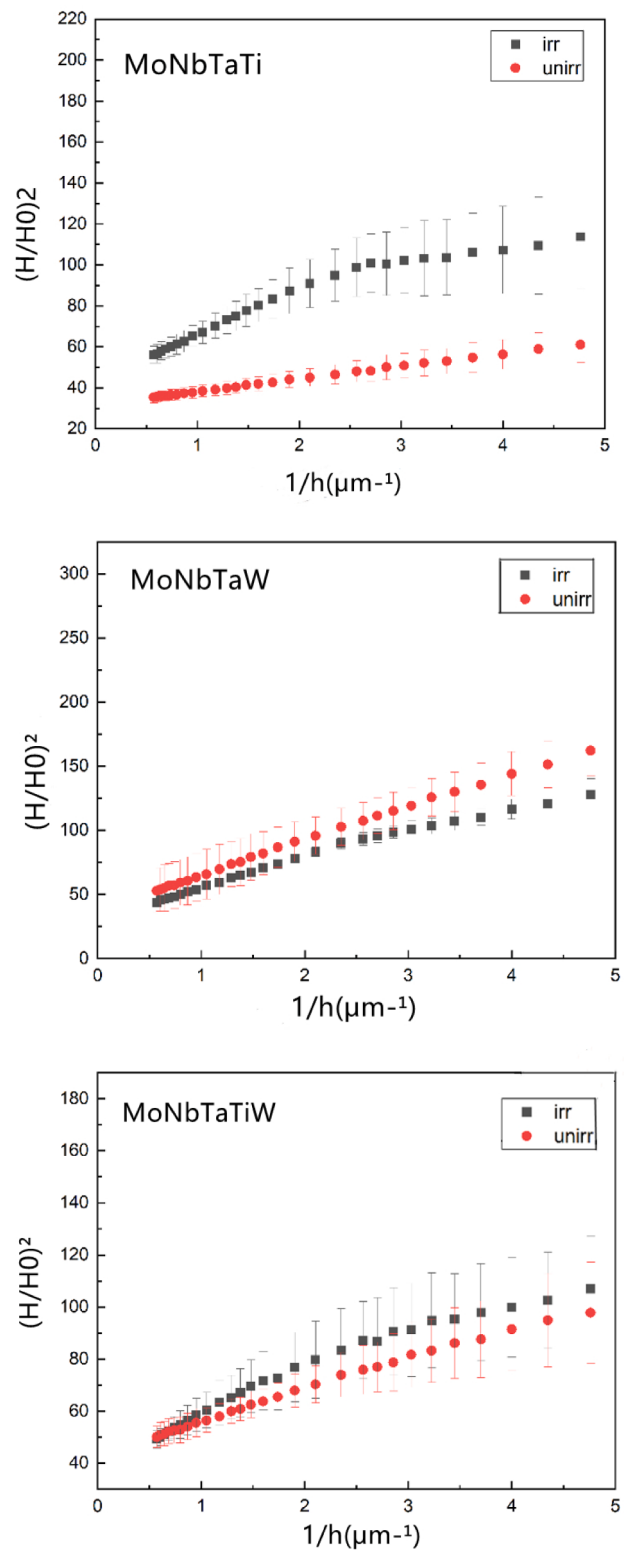


Fig. 10. Nix-Gao model for three HEAs after ion irradiation.

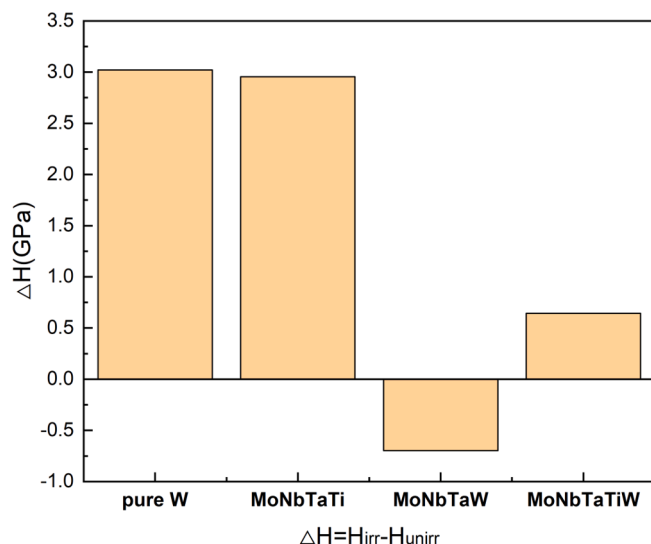


Fig. 11. Irradiation hardening of three BCC HEAs irradiated at 500°C and compare with pure.

Declaration of Competing Interest

The authors declare that they have no known competing financial interests or personal relationships that could have appeared to influence the work reported in this paper.

Acknowledgement

This work was supported by JSPS Grant-in-Aid for Scientific Research on Innovative Areas Grant Number JP21H00136.

References

- [1] J.W. Yeh, S.K. Chen, et al., Nanostructured High-Entropy Alloys with Multiple Principal Elements: Novel Alloy Design Concepts and Outcomes, *Advanced Engineering Materials* 6 (2004), 299303.
- [2] V. Dolique, A.L. Thomann, et al., Thermal stability of AlCoCrCuFeNi high entropy alloy thin films studied by in-situ XRD analysis, *Technology*. 204 (2010) 19891992.
- [3] M.-H. Tsai, C.-W. Wang, C.-W. Tsai, W.-J. Shen, J.-W. Yeh, J.-Y. Gan, W.-W. Wu, Thermal stability and performance of NbSiTaTiZr high-entropy alloy barrier for copper metallization, *Journal of the Electrochemical Society* 158 (11) (2011) H1161.
- [4] K.-Y. Tsai, M.-H. Tsai, J.-W. Yeh, Sluggish diffusion in Co–Cr–Fe–Mn–Ni high-entropy alloys, *Acta Materialia* 13 (2013) 4887–4897.
- [5] Y.u. Lei, N. Hashimoto, S. Isobe, Cu-Containing High Entropy Alloys for Nuclear Fusion Application, *Materials Transactions* 61 (7) (2020) 1247–1251.
- [6] K.R. Lim, K.S. Lee, et al., Dual-phase high-entropy alloys for high-temperature structural applications, *Journal of Alloys and Compounds* 728 (2017) 12351238.
- [7] X. Qiu, Microstructure and mechanical properties of CoCrFeNiMo high-entropy alloy coatings, *J. Mater. Microstructure and mechanical properties of CoCrFeNiMo high-entropy alloy coatings, Journal of Materials Research and Technology* 9 (3) (2020) 5127–5133.
- [8] R. Hahn, A. Kirnbauer, M. Bartosik, S. Kolozsvári, P.H. Mayrhofer, *Mater. Lett.* 251 (2019), 238240.
- [9] M.C. Gao, et al., The first-principles design of ductile refractory alloys, *Refractory Metals* 60 (2008) 61–65.
- [10] H.W. Yao, J.W. Qiao, J.A. Hawk, H.F. Zhou, M.W. Chen, M.C. Gao, Mechanical properties of refractory high-entropy alloys: Experiments and modeling, *Journal of Alloys and Compounds* 696 (2017) 1139–1150.
- [11] M.C. Gao, et al., Phase stability and elastic properties of Cr-V alloys, *Journal of Condensed Matter Physics* 25 (2013), 075402.
- [12] Zhang W, Liaw PK, Zhang Y. A Novel Low-Activation VCrFeTaxWx ($x = 0.1, 0.2, 0.3, 0.4$, and 1) High-Entropy Alloys with Excellent Heat-Softening Resistance. *Entropy*. 2018; 20(12):951.
- [13] S.Q. Wu, et al., Effect of Nb addition on microstructure and corrosion resistance of novel stainless steels fabricated by direct laser metal deposition, *Materials Research Express* 5 (2018), 036524.
- [14] X. Ye, B. Yang, Y. Nie, S. Yu, Y. Li, Influence of Nb addition on the oxidation behavior of novel Ni-base superalloy, *Corrosion Science* 185 (2021) 109436.
- [15] M.F. Montemor, et al., The role of Mo in the chemical composition and semiconductive behaviour of oxide films formed on stainless steels, *Corrosion Science* 41 (1999) 17–34.
- [16] O.N. Senkov, et al., Refractory high-entropy alloys, *Intermetallics* 18 (2010) 1758–1765.
- [17] H.Y. Diao, R. Feng, K.A. Dahmen, P.K. Liaw, Fundamental deformation behavior in high-entropy alloys: An overview, *Current Opinion in Solid State and Materials Science* 21 (5) (2017) 252–266.
- [18] Y.F. Ye, et al., Design of high entropy alloys: A single-parameter thermodynamic rule, *Scripta Materialia* 104 (2015) 53–55.
- [19] Y.F. Ye, et al., High-entropy alloy: challenges and prospects, *Materials Today* 19 (2016) 336–349.
- [20] Available at: <https://thermocalc.com/about-us/methodology/the-calphad-methodology/>.
- [21] M. Robinson, I. Torrens, Computer simulation of atomic-displacement cascades in solids in the binary-collision approximation, *Physical Review B* 9 (12) (1974) 5008–5024.
- [22] Available at: <http://www.srim.org>.
- [23] R.E. Stoller, M.B. Toloczko, G.S. Was, A.G. Certain, S. Dwaraknath, F.A. Garner, On the use of SRIM for computing radiation damage exposure, *Nuclear Instruments & Methods in Physics Research Section B* 310 (2013) 75–80.
- [24] W.C. Oliver, G.M. Pharr, An improved technique for determining hardness and elastic-modulus using load and displacement sensing indentation experiments, *Journal of Materials Research* 7 (6) (1992) 1564–1583.
- [25] Z. Zhang, E. Hasenhuettl, K. Yabuchi, A. Kimura, Evaluation of helium effect on ion irradiation hardening in pure tungsten by nano-indentation method, *Nuclear Materials and Energy* 9 (2016) 539–546.